Electronic Supplementary Material (ESI) for Dalton Transactions.

Solution Structure and Structural Rearrangement in Chiral Dimeric Ytterbium(III) Complexes Determined by paramagnetic NMR and NIR-CD

Moreno Lelli,*[a,b] Lorenzo Di Bari[c]

[a.] Department of Chemistry University of Florence. Via della Lastruccia 3, 50019 Sesto Fiorentino (FI), Italy. moreno.lelli@unifi.it
[b.] Centre of Magnetic Resonance (CERM), University of Florence, Via Luigi Sacconi 6, 50019 Sesto Fiorentino (FI), Italy.
[c.] Department of Chemistry and Industrial Chemistry, University of Pisa, Via Moruzzi 13, 56124, Pisa,Italy.

Table of Contents

Conformational Aspects in [Ln((S)-THP)] Complexes

The optical and magnetic properties of lanthanide–THP complexes depend on the geometry and the conformational dynamics of the ligand cage, we recall here the main structural aspects of the [Ln-((S)-H_4THP)] ligand cage. (S)-H_4THP is a chiral polydentate ligand analogous to the well-known lanthanide binding ligand DOTA (Scheme 1, main text). These ligands are octadentate, coordinating the metal through the 4 nitrogen atoms present in the macrocyclic cyclen ring, and the 4 oxygen atoms in the side arms.

With respect to DOTA, (S)-H_4THP is neutral with hydroxyl groups as oxygen donors, while in DOTA the coordination is provided by anionic carboxylates.

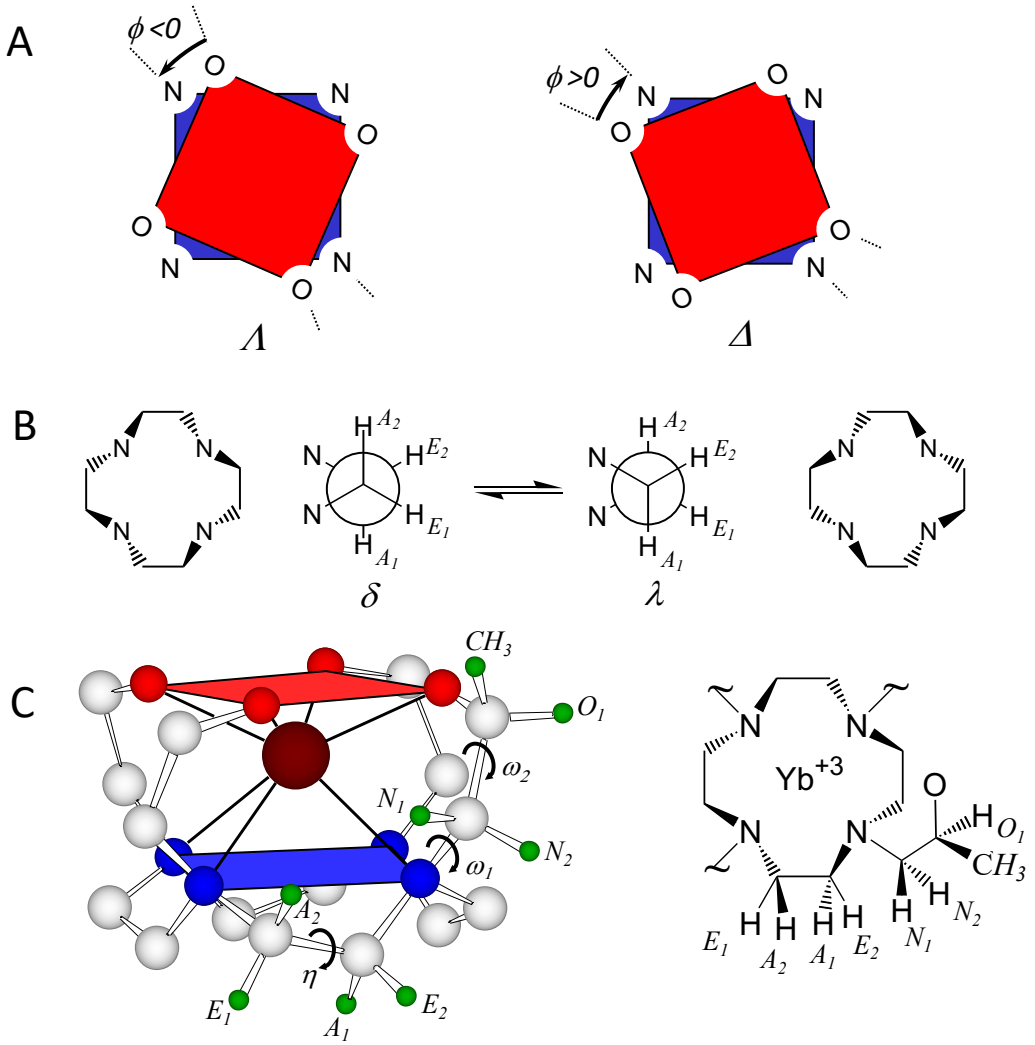

Figure S1. Schematic view of the ligand conformation in (S)-H_4THP (similar conformations are observed in several DOTA-like complexes). Panel A) Δ and Λ helicity of the side arm rotation. Panel B) ($\lambda,\lambda,\lambda,\lambda$) and ($\delta,\delta,\delta,\delta$) ring conformations. Panel C), assignment of the stereospecific hydrogen positions.

In lanthanide complexes of similar octadentatate ligands, a further 9th coordination site is possible in the axial position along the main C_4 symmetry axis. This additional axial coordination can be occupied typically by a solvent molecule or by water. Occupancy and exchange dynamics on this coordination site has profound effects on relevant properties of the Ln-complexes, including relaxivity (e.g. for the Gd(III) complex),[1] emission spectrum and lifetime (for Eu(III) and Tb(III) complexes),[2] magnetic susceptibility anisotropy (for most systems).[3]

In DOTA complexes, the ligand cage is not rigid in solution, but undergoes a series of conformational dynamics related to the flip of both the N–**C–C**–N ring dihedral or the C–**N–C**–C and the N–**C–C**–O side arm dihedrals (see Figure S1).[1,4–8] The combination of the ring and side arms conformations generates four possible stereoisomers: two enantiomeric couples of diastereosomers. The cyclen ring can assume the enantiomeric conformations ($\lambda,\lambda,\lambda,\lambda$) or ($\delta,\delta,\delta,\delta$) (Figure S1B), as well the side arms can have different twists with Λ or Δ chirality (Figure S1A). The coordination to the metal imposes the same conformation for all the ring dihedrals, mixed conformations, for example ($\lambda,\lambda,\delta,\delta$), are not possible. As well the side arms are oriented in a concerted fashion, with the same conformation for all the arms. The combination of these two chiral elements generates Square Antiprism (SAP, $\Delta(\lambda,\lambda,\lambda,\lambda)$ or $\Lambda(\delta,\delta,\delta,\delta)$) or Twisted Square Antiprism (TSAP, $\Lambda(\lambda,\lambda,\lambda,\lambda)$ or $\Delta(\delta,\delta,\delta,\delta)$) disteroisomers.[9,10] In $[Yb(DOTA)]^-$, the conformational dynamics in solution interconverts these stereoisomers. The two forms of SAP, namely $\Delta(\lambda,\lambda,\lambda,\lambda)$ and $\Lambda(\delta,\delta,\delta,\delta)$, are each other enantiomers and can interconvert each other by a conformational rearrangement. Similarly, the same is also valid for the two TSAP forms (i.e. $\Lambda(\lambda,\lambda,\lambda,\lambda)$ and $\Delta(\delta,\delta,\delta,\delta)$)).

In the absence of further stereogenic elements (for example in $[Yb(DOTA)]^-$), SAP is a *dynamic racemate* (i.e. the concentrations of $\Delta(\lambda,\lambda,\lambda,\lambda)$ and $\Lambda(\delta,\delta,\delta,\delta)$ are rigorously identical); similarly, for TSAP. On the other side, no symmetry relation exists between SAP and TSAP, which are usually differently populated, as a function of the specific ligand, of the Ln(III) ion, of the solution composition. Being disteroisomers, SAP and TSAP can have very different properties, like for example accessibility of the axial binding site and water exchange rate. The determination of the prevalent TSAP or SAP geometry in solution is generally not trivial, and tailored NMR study, eventually coupled with and CD techniques can be useful for this purpose.[9,10]

In the presence of an additional stereogenic element, like a chiral carbon atom either on the ring or on the side arm(s), the symmetry between the two SAP (or TSAP) enantiomers is broken and one of the two enantiomeric form of SAP or TSAP will prevail. This is the case of the [Yb((S)-H_4THP)]$^{3+}$ complex investigated here, where the chiral center in the sidearms imposes a discrimination between the two enantiomeric forms of each SAP and TSAP geometry.

In a previous study, we observed that the chiral centre in the (S)-H_4THP side arms blocks both sidearms and ring conformations: as consequence only one of the four possible TSAP and SAP stereoisomers of [Yb((S)-H_4THP)]$^{3+}$ is observed in solution. The analysis of the paramagnetic pseudocontact shifts and NIR-CD spectra made possible to determine that solution the geometry [Yb((S)-H_4THP)]$^{3+}$ is TSAP and the conformation is $\Delta(\delta,\delta,\delta,\delta)$.[9]

[As reported here and in Ref. 9 the correct conformation of [Yb((S)-H_4THP)]$^{3+}$ is TSAP and $\Delta(\delta,\delta,\delta,\delta)$. However in ref. 9, especially in the conclusions, is written an erroneous conformation because of a typographical error].

Paramagnetic NMR Structural Restraints in [Yb((*S*)-H_2THP)]$_2^{2+}$ Complex.

Paramagnetic Shift.

In a paramagnetic molecule, the observed NMR shift (δ_{obs}) is the sum of two contributions, a diamagnetic shift δ_{dia}, which can be estimated with an appropriate diamagnetic reference, and a paramagnetic shift δ_{para} which takes into account the effect of the hyperfine interactions.

$$\delta_{obs} = \delta_{dia} + \delta_{para} \quad \text{(S1)}$$

In turn, the paramagnetic shift includes the contribution of the Fermi contact shift (δ_{con}) and the pseudocontact shift (δ_{pc}, PCS), due to the long-range dipolar interaction.

$$\delta_{para} = \delta_{con} + \delta_{pc} \quad \text{(S2)}$$

In ytterbium complexes the contact shift contribution affects nuclei that are only a few bonds distant from the metal. Specifically for the [Yb((*S*)-H_4THP))]$^{3+}$ complex, it has been observed that for almost all the ^{1}H nuclei the contact contributions are indeed negligible with respect to the peudocontact terms, because all protons are at least three bonds away from the metal;[9] while it could have a modest contribution for carbons that are just two bonds form

the Yb(III) ion. It is reasonable to assume that also for the ^{1}H shift in the dimeric complex the paramagnetic contribution is essentially dominated by the pseudocontact shift. PCS is especially interesting for structural investigation, since it depends on the electron-nucleus dipolar interaction and it can be calculated knowing the position of the investigated nucleus with respect to the principal axes of the magnetic susceptibility tensor. In axially symmetric complexes (endowed with a symmetry axis of order equal or higher than C_3), PCS can be calculated as the product of a magnetic susceptibility anisotropy factor D, related to the anisotropy of the magnetic susceptibility tensor χ, and a geometrical factor $(3\cos^2\theta-1)/r^3$ that describes the position of the observed nucleus in the frame of the magnetic anisotropy tensor principal axes for the metal (eq. (S3)-(S4)).[1,11,12] Where r is the distance from the metal and θ is the polar angle describing the orientation of the r vector with respect to the main symmetry axis of the complex.

$$\delta_{pc} = D\left(\frac{3cos^2\theta-1}{r^3}\right) \quad \text{(S3)}$$

$$D = \frac{1}{12\pi}\left[\chi_{zz} - \left(\frac{\chi_{xx}+\chi_{yy}}{2}\right)\right] \quad \text{(S4)}$$

In the dimeric $[Yb((S)\text{-}H_2THP)]_2^{2+}$ complex the main principal axes of the magnetic susceptibility tensors of the two metals are collinear with the C_4 symmetry axis, which includes the positions of the two metal ions Yb(III) (Figure S2).

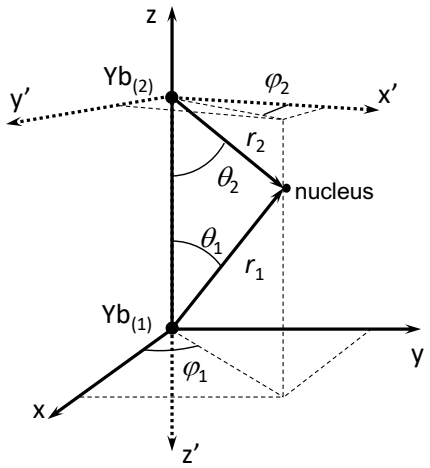

Figure S2. Schematic view of the orientation of the principal axes systems for the two metal ions in the dimeric head-to head complex.

Both the two paramagnetic Yb(III) ions affect the ^{1}H-NMR shifts and relaxation times. If the two ytterbium ions are sufficiently far away from each other to reasonably neglect their electron-electron coupling, the two paramagnetic centres can be considered as independent,[13] and each NMR-active nucleus receives paramagnetic contributions from each Yb ion.

Equations (S5)-(S6) describe the PCS in the dimer as the sum of the contribution coming from the two metals. The angles θ_1 and θ_2 are the polar angle with respect to the principal axis and r_1 and r_2 are the distances of the observed nucleus from the metals 1 and 2, respectively (Figure S2).

$$\delta_{pc} = D\left(\frac{3cos^2\theta_1 - 1}{r_1^3} + \frac{3cos^2\theta_2 - 1}{r_2^3}\right) \quad \text{(S5)}$$

$$D = \frac{1}{12\pi}\left[\chi_{zz} - \left(\frac{\chi_{xx} + \chi_{yy}}{2}\right)\right] \quad \text{(S6)}$$

For symmetry reasons the anisotropy of the magnetic susceptibility (D) is the same for both paramagnetic centres. In equation (S5) the unpaired spin density is assumed to be essentially localized on the metals, and the ^{1}H spins are sufficiently far from metals to be described within the limits of the point-dipole approximation, which is generally valid for Yb(III) complexes.[14]

Paramagnetic Relaxation Rates.

The nuclear relaxation times T_1 and T_2 are also largely affected by the presence of a paramagnetic centre. In analogy with NMR shift, also the relaxation rates (R_1, R_2, see equations (S7), (S8)) can be separated as the sum of a diamagnetic (R_1^{dia}, R_2^{dia}) and a paramagnetic contribution (R_1^{para}, R_2^{para}). The latter containing the effects of the contact, dipolar and Curie relaxation mechanisms.

$$R_1 = \frac{1}{T_1} = R_1^{dia} + R_1^{para} \quad \text{(S7)}$$

$$R_2 = \frac{1}{T_2} = R_2^{dia} + R_2^{para} \quad \text{(S8)}$$

The ^{1}H spins in these complexes are sufficiently far from the metal to neglect the contribution to relaxation due to the Fermi contact interaction. The paramagnetic relaxation rates are thus dominated by the dipolar (R_1^{dip}, R_2^{dip}) and Curie terms (R_1^{Curie}, R_2^{Curie}, equations

(S9)-(S10)). We see below that both these mechanism are related to the r^{-6} power of the distance of the observed nucleus from each Yb(III) ion.[11]

$$R_1^{para} = R_1^{dip} + R_1^{Curie} \quad \text{(S9)}$$

$$R_2^{para} = R_2^{dip} + R_2^{Curie} \quad \text{(S10)}$$

In particular, longitudinal relaxation times can be measured with good accuracy and is less affected than T_2 to conformational dynamics and scalar couplings. For this reason, it can be used to obtain structural information. Equations (S11) and (S12) describe the longitudinal relaxation time for the dimer for the two dipolar and Curie mechanisms in lanthanide complexes.

$$R_1^{dip} = \frac{2}{15}\left(\frac{\mu_0}{4\pi}\right)^2 \gamma_I^2 g_J^2 \mu_B^2 J(J+1)\left(\frac{7\tau_{e2}}{1+\omega_S^2\tau_{e2}^2} + \frac{3\tau_{e1}}{1+\omega_I^2\tau_{e1}^2}\right)\left(\frac{1}{r_1^6} + \frac{1}{r_2^6}\right) \quad \text{(S11)}$$

$$R_1^{Curie} = \frac{2}{5}\left(\frac{\mu_0}{4\pi}\right)^2 \frac{\gamma_I^2 g_J^2 \mu_B^4 B_0^2 [J(J+1)]^2}{(3kT)^2}\left(\frac{3\tau_R}{1+\omega_I^2\tau_R^2}\right)\left(\frac{1}{r_1^6} + \frac{1}{r_2^6}\right) \quad \text{(S12)}$$

Where γ_I is the nuclear gyromagnetic ratio, g_J is the lanthanide Landé factor, μ_0 is the vacuum magnetic susceptibility, μ_B is the Bohr magneton, B_0 is the magnetic field, J is the total electron angular momentum, k is the Boltzmann constant, and T the temperature. In particular for Yb(III) complexes the dipolar relaxation mechanisms is modulated by the electron correlation times (τ_{e1}, τ_{e2} ~10^{-13} s), while for the Curie relaxation mechanism, it is the molecular rotational correlation time (τ_R) that modulates the hyperfine interaction. Considering the symmetry of the dimer, all the constants and the correlation times are the same for both the paramagnetic centres and, neglecting cross-correlation terms the relaxation contributions of the two paramagnetic ions can be added together, for that reason in (S11) and (S12) the relaxation rates depends on both r_1 and r_2 which are the distances of the observed nucleus from the two Yb(III) ions, respectively.

Since both the Curie and dipolar relaxation rates, have the same spatial dependence, the overall paramagnetic longitudinal relaxation rate conserves the same dependence on r_1 and r_2 (eq. S13), where the constant k_1 group the ensemble of paramagnetic relaxation constants

and spectral densities for both mechanisms. Equation (S13) shows us that the paramagnetic relaxation rates can be used as restraint for the structural determination of the dimer.

$$R_1^{para} = R_1^{dip} + R_1^{Curie} = k_1\left(\frac{1}{r_1^6} + \frac{1}{r_2^6}\right) \quad \text{(S13)}$$

Experimental Part

NMR Assignment Procedure.

The ^{1}H NMR methyl resonance was easily assigned in the NMR spectrum on the basis of the resonance integrals. The other proton resonances were assigned on the bases of a 2D COSY QF spectrum and by comparison with the monomer assignment to solve some residual ambiguity. In such a way, it was possible to unambiguously assign all the ^{1}H resonances unless the stereospecific assignment of the N_1 and N_2 protons. Their stereospecific assignment was fixed within the structural calculation, with a procedure similar to those used in conventional protein NMR structural calculation. Different PERSEUS calculations were run with both the two possible stereospecific N_1 and N_2 assignments for each of the two investigated cases: rearranged and not rearranged ligand cage. The different N_1 and N_2 assignments lead to different calculated geometries, the wrong assignment was discarded because it gives a too poor values for the quality factor or an unacceptable arrangement of the side arm conformation keeping the oxygen donor atoms too far from the coordinated Yb(III) ion.

The resonances of the lutetium complex [Lu((S)-H_4THP)]$^{3+}$,[15] were used as diamagnetic reference for the determination of the dimeric ^{1}H NMR paramagnetic shifts with equation (S1). The differences in the diamagnetic shifts between dimeric and monomeric forms is expected to be minimal, and negligible with respect to the paramagnetic contribution. To determine the paramagnetic contribution to the longitudinal relaxation rates (eq.(S7)), the experimental relaxation rates were subtracted of the diamagnetic relaxation rate estimate to be 1.0 s^{-1}.

PERSEUS NMR Analysis Routine.

PERSEUS is the software used for the determination of the structure of the dimer in solution. Details in the PERSEUS routine can be found in ref. 16. The PERSEUS routine uses paramagnetic

NMR shifts and relaxation times as structural restrains for the structural determination. Distance restrains, and in particular restraining the distance of the ligand donor atoms to the metal can be introduced in the structural optimization, but this kind of restrain was not used in the present calculation. PERSEUS start with an initial, not refined, structural model and initial values for the magnetic parameters to calculate PCS and relaxation rates through equations (S5), (S13). Then, it starts to optimize the magnetic parameters (the magnetic susceptibility anisotropy factor D, the orientation of the principal tensor axes, the relaxation constant k_1) as well modifying the initial three dimensional structure, for example changing the position of the two Yb(III) ions and the side arms conformations in order to minimize the target function *F*.

$$F = \frac{\sum_i A_i\left(\delta_i^{exp} - \delta_i^{calc}\right)^2}{\sum_i\left(\delta_i^{exp}\right)^2} + \frac{\sum_j B_j\left(R_j^{exp} - R_j^{calc}\right)^2}{\sum_j\left(R_j^{exp}\right)^2}$$

F measures the distance between the calculated (δ^{calc}) and experimental shifts (δ^{exp}) as well as the experimental (R^{exp}) and calculated relaxation rates (R^{calc}). The relative importance of the two kinds of restraints is weighted by the factors A_i and B_j. The final structure will have the geometry that minimizes the target function, thus it will be in a good agreement between the calculated and experimental paramagnetic restraints.

The quality of the optimization is measured by the quality factors Q(δ_{pc}) and Q(R_1). Defined in analogy with the Willcott's agreement factor:[17,18]

$$Q(\delta_{pc}) = \sqrt{\frac{\sum_i A_i\left(\delta_i^{exp} - \delta_i^{calc}\right)^2}{\sum_i\left(\delta_i^{exp}\right)^2}}$$

$$Q(R_1) = \sqrt{\frac{\sum_i B_i\left(R_{1,i}^{exp} - R_{1,i}^{calc}\right)^2}{\sum_i\left(R_{1,i}^{exp}\right)^2}}$$

As described in the main text, two kinds of PERSEUS calculations were run: in the first case we kept the molecular geometry rigid conserving the position that where optimized in solution structure reported in ref. 9. This optimization was done optimizing only the magnetic parameters (magnitude and orientation of the magnetic anisotropic tensors and the longitudinal relaxation constant k_1) and the relative position of the two Yb(III) ions. In the second calculation, in addition to the magnetic parameters, PERSEUS optimizes also the molecular geometry: in particular the side arms conformations (the angles ω_1 and ω_2 in

Figure S1) and the position of both Yb(III) atoms were adjusted to fit the experimental data. The ring conformation (η angle, Figure S1) was optimized by repeating the PERSEUS calculations on a series of starting models where the ring dihedral was modified with a molecular mechanic software (CS CHEM 3D PRO 3.5.2. Cambridge, MA: Cambridge Soft Corporation); than selecting the final structure producing the smaller target function *F*.

Dimer ESI MS Spectra.

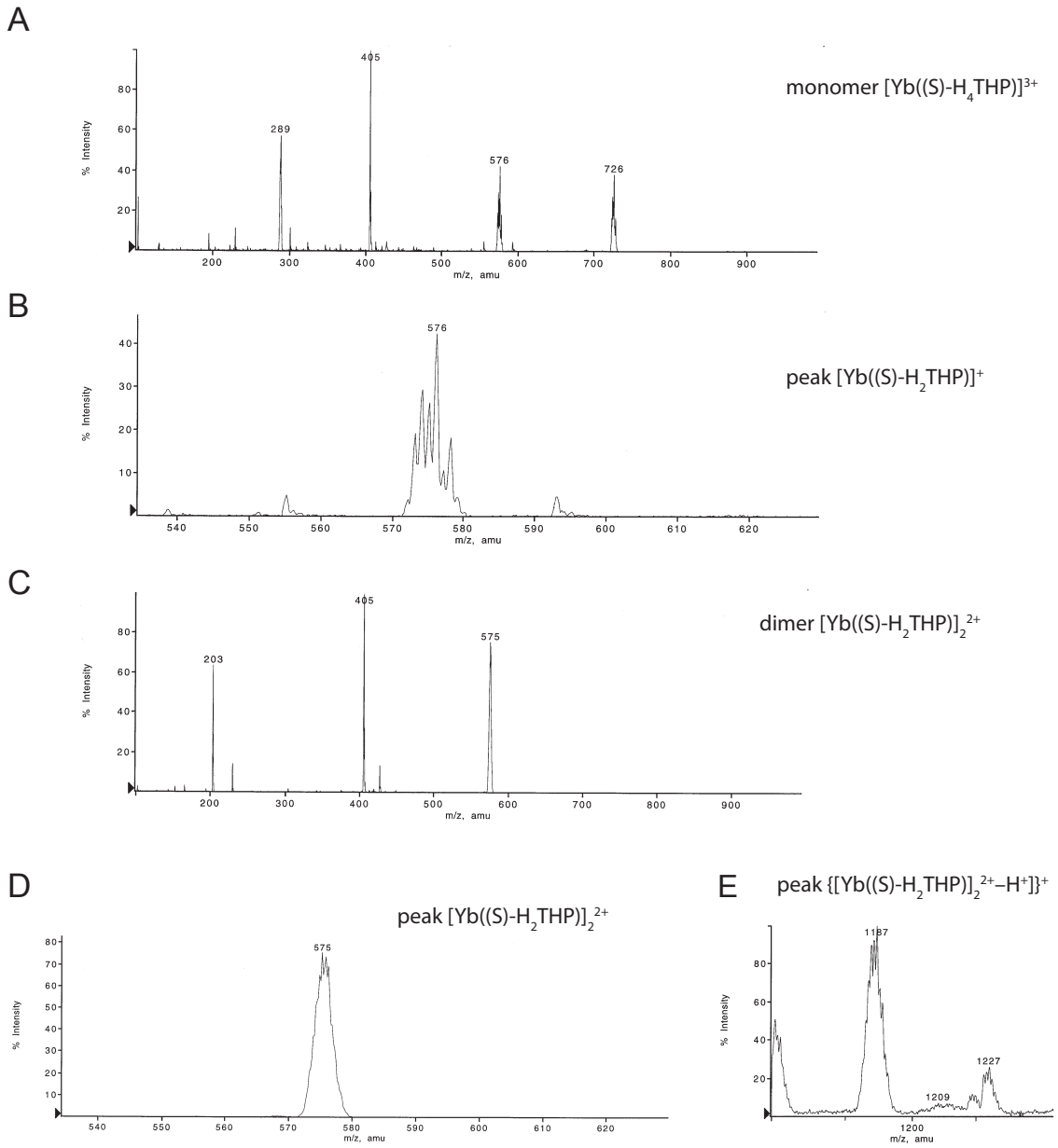

Figure S3. ESI MS spectra of the $[Yb((S)\text{-}H_4THP)]^{3+}$ monomer and dimer ($[Yb((S)\text{-}H_2THP)]_2^{2+}$) in CH_3CN. Panel A: monomeric $[Yb((S)\text{-}H_4THP)]^{3+}$ in CH_3CN, B) enlargement of the monocharged peak at 576 a.m.u. of $[Yb((S)\text{-}H_2THP)]^{+}$. C) Spectrum of the dimeric $[Yb((S)\text{-}H_2THP)]_2^{2+}$ obtained from the $[Yb((S)\text{-}H_4THP)]^{3+}$ solution after addition of Et_3N. D) enlargement of the peak at 576 a.m.u. corresponding to the di-charged species $[Yb((S)\text{-}H_2THP)]_2^{2+}$, and E) the monocharged peak of $\{[Yb((S)\text{-}H_2THP)]_2^{2+}–H^+\}^+$. In panel E the vertical scale has been expanded to make visible the peak of $\{[Yb((S)\text{-}H_2THP)]_2^{2+}–H^+\}^+$. Indeed, it is very weak and not observable if plotted with the same scale level of panel C and D.

References

1 S. Aime, M. Botta, Z. Garda, B. E. Kucera, G. Tircso, V. G. Young and M. Woods, *Inorg. Chem.*, 2011, **50**, 7955–7965.
2 D. Parker, *Chem. Soc. Rev.*, 2004, **33**, 156.
3 J. Luzon and R. Sessoli, *Dalt. Trans.*, 2012, **41**, 13556.
4 S. Aime, M. Botta and G. Ermondi, *Inorg. Chem.*, 1992, **31**, 4291–4299.
5 G. Tircso, B. C. Webber, B. E. Kucera, V. G. Young and M. Woods, *Inorg. Chem.*, 2011, **50**, 7966–7979.
6 K. J. Miller, A. A. Saherwala, B. C. Webber, Y. Wu, A. D. Sherry and M. Woods, *Inorg. Chem.*, 2010, **49**, 8662–8664.
7 P. Salvadori and L. Di Bari, in *Organometallic Chirality*, eds. G. Pàlyi, L. Caglioti and C. Zucchi, Mucchi Editore, Modena, 2008, pp. 227–246.
8 V. Jacques and J. F. Desreux, *Inorg. Chem.*, 1994, **33**, 4048–4053.
9 M. Lelli, G. Pintacuda, A. Cuzzola and L. Di Bari, *Chirality*, 2005, **17**, 201–211.
10 L. Di Bari, G. Pintacuda and P. Salvadori, *Eur. J. Inorg. Chem.*, 2000, 75–82.
11 I. Bertini, C. Luchinat and G. Parigi, *Solution NMR of Paramagnetic Molecules*, Elsevier, Amsterdam, 2001.
12 I. Bertini, C. Luchinat and G. Parigi, *Prog. Nucl. Magn. Reson. Spectrosc.*, 2002, **40**, 249–273.
13 I. Bertini and C. Luchinat, *Coord. Chem. Rev.*, 1996, **150**, 1–300.
14 R. M. Golding, R. O. Pascual and B. R. McGarvey, *J. Magn. Reson.*, 1982, **46**, 30–42.
15 K. O. A. Chin, J. R. Morrow, C. H. Lake and M. R. Churchill, *Inorg. Chem.*, 1994, **33**, 656–664.
16 L. Di Bari, G. Pintacuda, S. Ripoli and P. Salvadori, *Magn. Reson. Chem.*, 2002, **40**, 396–405.
17 M. R. Willcott, R. E. Lenkinski and R. E. Davis, *J. Am. Chem. Soc.*, 1972, **94**, 1742–1744.
18 R. E. Davis and M. R. Willcott, *J. Am. Chem. Soc.*, 1972, **94**, 1744–1745.
19 E. Babini, I. Bertini, F. Capozzi, I. C. Felli, M. Lelli and C. Luchinat, *J. Am. Chem. Soc.*, 2004, **126**, 10496–10497.
20 S. Balayssac, I. Bertini, M. Lelli, C. Luchinat and M. Maletta, *J. Am. Chem. Soc.*, 2007, **129**, 2218–2219.
21 S. Balayssac, I. Bertini, A. Bhaumik, M. Lelli and C. Luchinat, *Proc. Natl. Acad. Sci.*, 2008, **105**, 17284–17289.
22 I. Bertini, A. Bhaumik, G. De Paëpe, R. G. Griffin, M. Lelli, J. R. Lewandowski and C. Luchinat, *J. Am. Chem. Soc.*, 2010, **132**, 1032–1040.
23 I. Bertini, L. Emsley, M. Lelli, C. Luchinat, J. Mao and G. Pintacuda, *J. Am. Chem. Soc.*, 2010, **132**, 5558–5559.
24 L. Di Bari, M. Lelli, G. Pintacuda, G. Pescitelli, F. Marchetti and P. Salvadori, *J. Am. Chem. Soc.*, 2003, **125**, 5549–5558.
25 J. Lisowski, S. Ripoli and L. Di Bari, *Inorg. Chem.*, 2004, **43**, 1388–1394.